Statistical analysis of correlations and intermittency of a turbulent rotating column in a magnetoplasma device

S. Magni,[1] H. E. Roman,[1] R. Barni,[1] C. Riccardi,[1] Th. Pierre,[2] and D. Guyomarc'h[2]
[1]*Dipartimento di Fisica, Universitá di Milano-Bicocca, Piazza della Scienza 3, 20126 Milano, Italy*
[2]*Laboratoire PIIM, CNRS et Université de Provence, 13397 Marseille, France*
(Received 10 March 2005; revised manuscript received 6 June 2005; published 5 August 2005)

A statistical analysis of density fluctuations in a cylindrical nonfusion device is performed. The experimental setup is implemented in order to reach a turbulent behavior of the linear plasma column. Two different turbulent regimes are obtained corresponding to two selected sets of values for the discharge parameters. The first regime displays a rotating column characterized by the presence of a shear layer separating the plasma bulk from the tenuous plasma in the shadow of the limiter, the latter showing a strong intermittent behavior and superdiffusion. The second regime corresponds to a weakly rotating column in which coherence is lost in the plasma bulk and a standard diffusive process takes place in the shadow region. These findings are supported by the calculation of the Hurst's exponent using wavelet-analysis techniques. Furthermore the intermittent behavior is characterized and related to the diffusive process. Finally the shape of the probability distribution function of density fluctuations seems to be well described by an analytical form suggested on the basis of Tsallis generalized statistics.

DOI: 10.1103/PhysRevE.72.026403 PACS number(s): 52.35.Ra, 52.35.Mw, 52.25.Gj

I. INTRODUCTION

The study of turbulence in nonfusion plasma devices is an important task to assess the understanding of transport in more complex, large-scale plasma configurations. Early measurements have exhibited turbulent fluctuations of the plasma density in laboratory devices [1]. It was soon recognized that the study of drift instabilities is basic to the understanding of anomalous transport in fusion devices. For instance, the effect of temperature gradient, sheath resistivity, and density gradient was studied in Q machines [2–5].

Recently, features like long-time correlations [6–8], super-diffusive behaviors [9], and non-Gaussian distributions [10–12] of the plasma density fluctuations are commonly observed in these fusion devices. Many theoretical attempts have been developed to relate these characters to intermittent transport [13–16]. From an experimental point of view, time series obtained by different plasma-diagnostic techniques have been examined using different statistical tools [6–9,17–19].

In this paper, a detailed analysis of electronic density fluctuations in the cylindrical non-fusion device Mistral [20] is presented. The experimental setup is implemented in order to obtain a turbulent regime in a rotating plasma column. Adjusting the boundary conditions, one can experimentally control the speed of the rotation. In this work we consider two distinct sets of control parameters, corresponding to the anode potential and the biasing of the collecting plate achieving two distinct turbulent regimes.

The different morphologies of turbulent transport, obtained only by means of different rotations of this cold plasma column, can be an important contribution to understand the transport phenomenology at the border of the tokamak, where fast shear layers are present. In particular we want to point out the importance of centrifugal effects [21], rarely taken into account in modeling.

The paper is organized as follows. Section II is devoted to a description of the experimental setup employed, and Sec. III is a discussion of the results. The latter includes several statistical tools to study the moments of the fluctuating signals, such as mean value, standard deviation, skewness, and flatness, as a function of the radial distance r from the center of the cylindrical device (Sec. III A). The calculation of Hurst's exponent and the characterization of the intermittency is presented in Sec. III B. An analytical form of the probability distribution function (PDF), suggested on the basis of Tsallis generalized statistics, is provided and discussed in relation to the experimental data (Sec. III C). Finally, Sec. IV contains the concluding remarks.

II. EXPERIMENTAL SETUP

A schematic diagram of the Mistral device is depicted in Fig. 1. It is made up of three main parts: (i) a large stainless steel vacuum chamber (70 cm radius, 100 cm length) where the neutral gas (argon) is injected and the pumping system is connected; (ii) a metallic cylinder (20 cm radius, 120 cm length) surrounded by 50 equally spaced water-cooled coils setting up a solenoid producing a magnetic field up to 0.04 T; and (iii) a semitoroidal chamber (main radius 60 cm, 20 cm minor radius) which is however disconnected in the experiment here reported. The semitoroidal chamber is thought to study the instabilities induced by the curvature of the magnetic field.

The plasma is produced by a large multipolar source, in a configuration derived from the experiment Mirabelle [22]. It consists of 32 tungsten filaments (0.2 mm diameter, 15 cm length) heated at 2100 K and disposed on one side of the main chamber along with two concentric circles. The ionizing electrons are extracted by an anodic grid which covers the remaining part of the chamber, insulated from the latter. About 1000 ferrite magnets are distributed uniformly all over

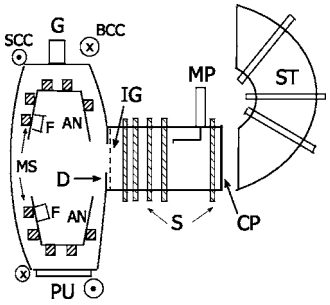

FIG. 1. The scheme of the mistral device (top view). The large multipolar source (left), the linear part (middle), the disconnected semitorus (ST—right). MS: ferrite magnets; F: hot filaments; AN: anodic grid; G: gas injection; PU: pumping system; BCC: big compensation coil; SCC: small compensation coil; S: solenoid; D: diaphragm; IG: injection grid; CP: collecting plate; MP: scanning Langmuir probe.

the grid creating little magnetic cusps enhancing the plasma density and spatially smoothing its profile. A pair of asymmetric compensation coils lies outside the chamber. They have a polarity opposite to that of the solenoid and produce a magnetic cusp 20 cm in front of the cathode plane.

A high transparency grid is inserted between the source chamber and the linear one, and kept floating. In these experiments, the plasma has been confined to the linear part of the chamber by a circular biased collector. The plasma diameter is limited to 12 cm by a metallic diaphragm (annular limiter), placed at the entrance of the cylinder. In this way, diffusion can be investigated in the shadow of the limiter where the ionization process is no longer present.

Only primary electrons overcome the floating potential of the injection grid and ionize the gas filling the tube. A negative charge surplus is created close to the axis of the latter, while the ions are poorly magnetized and contribute to a radial loss of charges outside the plasma column. A radial equilibrium electric field **E** then sets in, having axial symmetry. Electrons and ions drift in the same direction at the same $\mathbf{E}\times\mathbf{B}$ velocity, contributing to the rotation of the column.

With the grid kept floating, the control parameters are the potential of the anode V_A and the biasing of the collecting plate V_{plate}. A pronounced rotation of the column, due to the resulting electric field **E**, stabilizes the plasma bulk but triggers low frequency coherent waves. The $m=2$ poloidal mode was characterized previously in Ref. [23]. One can observe a $m=2$ mode for $V_{\text{plate}}=30$ V going through a $m=1$ mode gradually lowering the value of V_{plate}. The turbulence behavior appears for $V_{\text{plate}}\leqslant 20$ V (see Ref. [20] for more details). The anodic potential is consequently tuned to obtain a stationary discharge. The values corresponding to the turbulent regime A and B, together with the amplitude of the external magnetic field B_S are reported in Table I. In regime A, the column rotates almost rigidly and structures develop at the edge with the ejection of plasma density blob which evolves in a spiral arm before fading away [20]. In regime B, the column itself is interested by turbulence showing strong density fluctuations.

The neutral pressure was kept at 2×10^{-2} Pa. The mean plasma parameters are the following: $n_e=(10^{14}$–$10^{16})$ m^{-3}; $T_e=(2$–$4)$ eV; ions remain cold ($T_i\leqslant 0.1$ eV). The electronic saturation current is measured through a cylindrical Langmuir probe, with a polarization of 18 V. An automated acquisition system is adopted, where the stepper-motor of the movable probe and the oscilloscope are managed by a LAB VIEW® program.

TABLE I. The two sets of control parameters for the two turbulent regimes here investigated: anodic grid potential V_A, bias potential of the collecting plate V_{plate}, magnetic field B_S generated by the external coils at the center of the cylindrical chamber.

Regime	V_A(V)	V_{plate}(V)	B_S(T)
A	−8	18	1.6×10^{-2}
B	−3	10	1.6×10^{-2}

We study stationary time records of length $N=5\times10^4$, representing electron density fluctuations (disregarding electron temperature fluctuations) at position r from the center of the cylindrical device, taken at the time-sampling Δt. Both ac and dc signals have been considered. For regime A, we have taken $\Delta t=2$ μs and obtained 20 series per radial position for dc signals, and 100 series per radial position for ac signals. For regime B, we have taken $\Delta t=4$ μs and obtained 50 series per radial position for both dc and ac signals. The results presented are thus based on large statistics, which correspond to 6×10^6 events for regime A and 5×10^6 for regime B.

III. RESULTS

We study electron density fluctuations $\tilde{n}_e(r,t)=n_e(r,t)-\langle n_e(r)\rangle$, where $\langle n_e(r)\rangle$ is the mean value at r, and calculate few higher moments of $\tilde{n}_e(r,t)$, such as the standard deviation, $\sigma_n=\langle\tilde{n}_e^2\rangle^{1/2}$, which measures the amplitude of fluctuations, the skewness, $S=\langle\tilde{n}_e^3\rangle/\sigma_n^3$, which measures the asymmetry of the signal, and the flatness $F=\langle\tilde{n}_e^4\rangle/\sigma_n^4$, which roughly tells us about the presence of extremal events. Adhering to plasma turbulence terminology, they are called intermittent bursts and are responsible for fat-tailed PDFs. The kurtosis, sometimes reported in literature instead of the flatness, is related to it by $K=F-3$. For comparison, the Gaussian (or normal) distribution has $S=0$ and $F=3$ (i.e., $K=0$).

The type of signals we are considering here are illustrated in Fig. 2. They correspond to two selected radial positions which are found to be paradigmatic of the turbulent behavior observed in the two regimes considered. One can notice a clear difference in the morphology of the signals. Our goal is to characterize the latter using standard statistical tools.

To this end, we start by considering the first four moments of the corresponding density fluctuations distributions along the whole range of radial positions for both regimes. In this way we are able to localize those regions displaying the strongest fluctuations and intermittency. A key quest is, next, whether the signals have long-time autocorrelations, which can be answered by accurately determining the Hurst's exponents. Regarding the question of intermittency, we shall investigate the bursts statistics (shape and waiting time distributions) which can shed some light onto the underlying

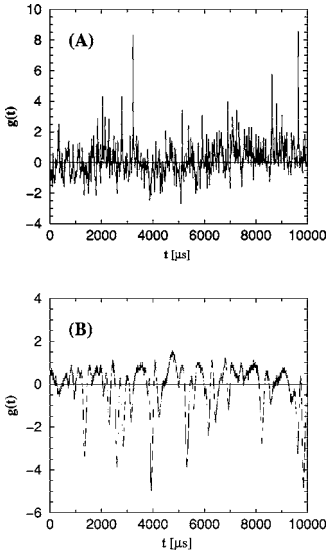

FIG. 2. Electron density fluctuations plotted in its scaled form $g(t)=\tilde{n}_e(r,t)/\sigma_n$, displaying intermittent behavior, for two selected radial positions: (A) Regime A for $r=10.5$ cm and (B) regime B for $r=3.5$ cm.

intermittent mechanisms. Finally, we will consider the overall shape of the density fluctuations PDF, in particular regarding the distribution of extremal events (the peaks in Fig. 2). The shapes discussed here can be confronted with those already suggested in the literature in other devices.

A. Moments of the PDF and phenomenology

Regimes A and B seem to display two different phenomenologies. In Figs. 3 and 4, the mean electron density $\langle n_e(r)\rangle$ and relative fluctuations, $\sigma_n(r)/\langle n_e(r)\rangle$, are plotted as a function of radial position r. In the figures, also the position of the diaphragm (limiter) is indicated.

A steep density gradient can be observed in both cases at the border of the limiter, where a shear layer exists. In the shadow of the limiter there are no ionizations. In the latter, however, the plasma is carried by some instabilities and by turbulent transport as it happens in the edge, namely, the scrape-off layer (SOL), of the larger fusion devices. We can

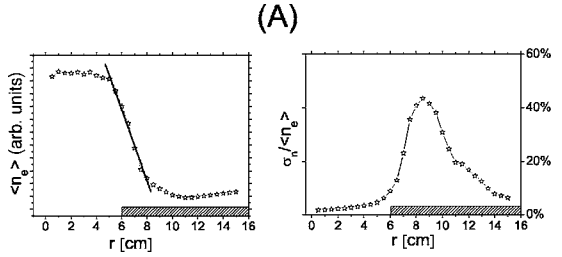

FIG. 3. Mean value $\langle n_e(r)\rangle$ (left) and relative fluctuations $\sigma_n/\langle n_e(r)\rangle$ (right) of electron density signal as a function of distance r for regime A. The position of the limiter ($6\ \text{cm}\leqslant r\leqslant 20$ cm) is indicated by the shadowed bar. A linear fit (straight line) around $r=6$ cm is also shown to underline the fast density gradient occurring in going from the plasma bulk toward the shadow of the limiter.

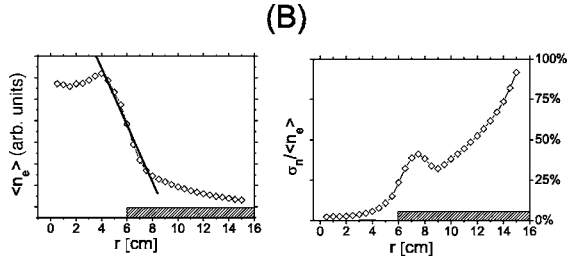

FIG. 4. Mean value $\langle n_e(r)\rangle$ (left) and relative fluctuations $\sigma_n/\langle n_e(r)\rangle$ (right) of electron density signal as a function of distance r for regime B. The position of the limiter ($6\ \text{cm}\leqslant r\leqslant 20$ cm) is indicated by the shadowed bar. A linear fit (straight line) around $r=6$ cm is also shown.

therefore call the shadow of the diaphragm the edge region. The absolute values of density in the plasma bulk (not reported here) reduce up to 60 % passing from cases A to B. The relative fluctuations reach a maximum at the edge of the diaphragm but in case B they grow indefinitely to the walls.

In case A, a closer look at the higher moments (Fig. 5) reveals that fluctuations display a nearly-Gaussian character, except for a very narrow region in the middle of the edge region ($9\ \text{cm}\leqslant r\leqslant 11$ cm) where a high intermittency emerges. The behavior of the plasma in this regime closely resembles the one described in Ref. [20].

The large level of fluctuations observed in this region (cf. top of Fig. 2), and the pedestal density profile of Fig. 3 displayed just outside the limiter, are thought to be due to the passage of a plasma structure developing there. In this small region, fluctuations are dominated by bursts in which a large fraction of the density, typically visualized as an arm of a spiral, can sometimes detach giving rise to large density blobs. In particular, strong radial $\mathbf{E}\times\mathbf{B}$ velocities have been measured by an enhanced conditional sampling technique inside such a structure, indicating that a convective transport takes place there [20]. The level of radial velocity approaches the rotation rate (the poloidal velocity) as displayed in Fig. 6. For $r>8$ cm, the radial velocity of the structure exceeds the poloidal one, pointing out to a plasma transport outside the limiter. We will see below how these fluctuations modify the diffusion behavior in the nearby zones.

In regime B, we distinguish essentially two zones: the plasma core ($r\leqslant 7$ cm) where now intermittency is present

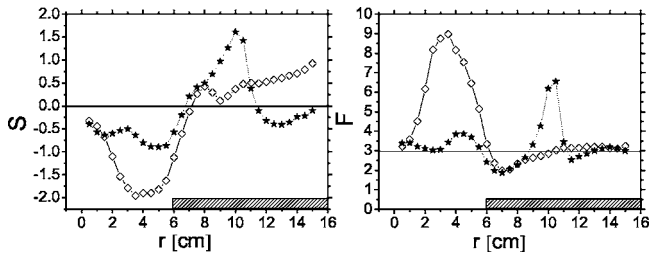

FIG. 5. Different moments of density fluctuations as a function of distance r: skewness S (left), flatness F (right). Regime A (black stars), regime B (open diamonds). The position of the limiter ($6\ \text{cm}\leqslant r\leqslant 20$ cm) is indicated by the shadowed bar. The horizontal lines indicate the values corresponding to a normal distribution and are included as a reference.

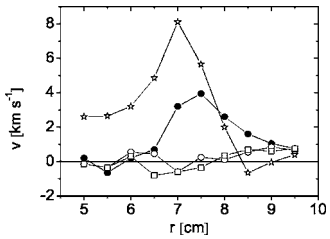

FIG. 6. Radial profile of the $\mathbf{E}\times\mathbf{B}$ velocity. The symbols represent: (full circles) the radial velocity inside the plasma structure, (open circles) the radial velocity measured 20 μs before the passage of the structure, (open squares) the radial velocity measured 20 μs after the passage of the structure, and (stars) the poloidal velocity.

(Fig. 5) making the column lose part of its coherence; the edge region ($r>7$ cm) in which the plasma displays a normal behavior. In this second case a picture of possible coherent turbulent structures is still not available.

Roughly speaking, fluctuations in regime A resemble a tokamak configuration, where turbulence is restricted to the edge region and the bulk is rotating nearly as a rigid body [10,24]. Regime B seems closer to a simple magnetized torus, where a strong intermittency is present in the inner part of the vacuum chamber and it is strictly correlated to plasma production [19,25]. In the following, we study in some detail the statistics of fluctuations for the two radial positions: $r=10.5$ cm for regime A and $r=3.5$ cm for regime B. These radial locations correspond to the positions of the peaks observed in Fig. 5 for the flatness.

B. Hurst's exponents and statistics of intermittency

The Hurst (H) exponents have been estimated using wavelet analysis up to third-order (see Appendix for more details). In Fig. 7 a comparison is shown between the first three orders for the two selected radial positions. One can see the time scales over which power-law behaviors are observed. Generally they cover (1.5–2) decades corresponding to the time scale (10^2–5×10^4) μs.

The results for H versus radial position, corresponding to third-order wavelets are reported in Fig. 8. For regime A (left panel), fluctuations display $H\approx1$ (ballistic diffusion) in the hole of the limiter ($r\leqslant6$ cm), a consequence of the fact that

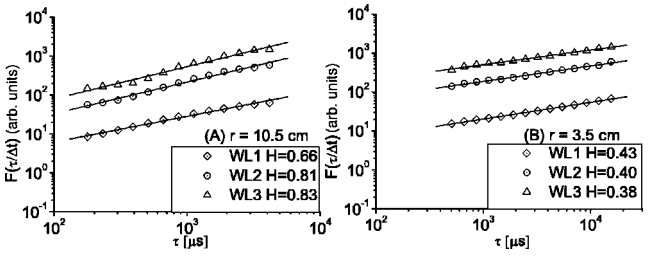

FIG. 7. Estimation of the Hurst exponent for regime A at $r=10.5$ cm (left) and regime B at $r=3.5$ cm (right). The comparison between first-order wavelet $F_1(\ell)$ (WL1: open diamonds), second-order wavelet $F_2(\ell)$ (WL2: open circles), and third-order wavelet analysis $F_3(\ell)$ (WL3: open triangles) is shown. Here, $\ell=\tau/\Delta t$. The resulting values of H are reported in the insets.

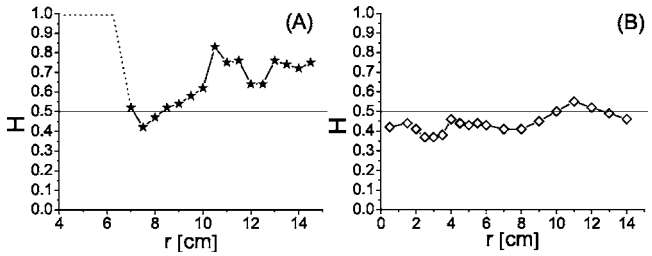

FIG. 8. Hurst's exponents for regime A (left) and B (right), as a function of radial distance r, obtained using third-order wavelet analysis, $F_3(\ell)$, Eq. (A5).

the plasma rotates as a quasirigid body. Close to its border ($6\text{ cm}<r<9$ cm), we find H=(0.45–0.55) corresponding to standard diffusion. In the intermittent zone ($9\text{ cm}\leqslant r\leqslant11$ cm), H=(0.75–0.83) pointing to a super-diffusive situation consistent with the pictures of expelled blobs of density. This is consistent with the results shown in Fig. 6 in which the radial velocity exceeds the poloidal one, leading to a persistence of fluctuations in this region of the chamber. Finally, for $r>11$ cm, H=(0.65–0.75) corresponding to a weaker super-diffusive behavior. This can be interpreted as a residual diffusive process which keeps memory of turbulent convection from the above mentioned detached structures.

For regime B (see Fig. 8, right panel), we have a slightly antipersistent signal with H=(0.38–0.45) within the hole of the limiter up to $r=9$ cm. These long-time anti-correlations can be ascribed to the plasma source. Similar anomalies (i.e., $H\neq1/2$) have been recently reported for the inner zone of a thoroidal magnetoplasma where the hot-cathode discharge is located [26,27].

For $r>9$ cm, we find $H\approx0.5$ (standard diffusion) well behind the shadow of the limiter. In this case, we can exclude super-diffusive behavior due to a Lévy-like process being the corresponding PDF close to Gaussian (not shown here). In regime A, we have pointed out that the presence of coherent structures can explain the observed super-diffusion. In this second case, it is resonable to ask whether standard diffusion is a result of the lack of such structures. The answer to this question cannot be affirmative in general. There are known cases in literature where vortexlike coherent structures of a cold turbulent plasma are accompanied by standard diffusion (see e.g., [26,28]).

In addition to H, the intermittency in the same time series can be investigated by means of recently-reviewed statistical tools [11,18]. We have considered the question of identifying the shape of bursts in the signals. To do this, a burst is defined as a fluctuation which overcomes the threshold $\pm3\sigma_n$, and perform an average over all such events within the time series corresponding to a particular position r. The sign of the threshold is chosen on the basis of the sign of the skewness S.

Results for the burst shapes obtained for position $r=10.5$ cm for regime A, and for $r=3.5$ cm for regime B, are shown in Fig. 9. For regime A, a "typical" positive burst is observed (see Fig. 5 in [18]), while in regime B the large events are negative. We could use the standard term "hole," in this second case. Note also the different shapes and widths

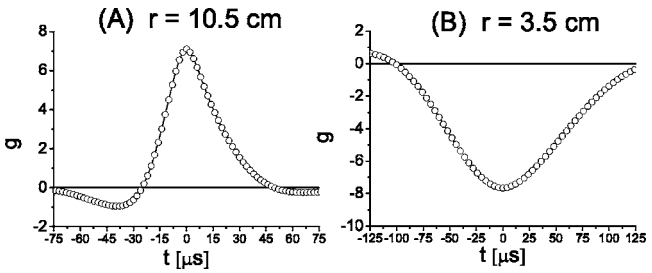

FIG. 9. The average shape of bursts of scaled density fluctuations $g \equiv \tilde{n}_e/\sigma_n$ versus time lag $t[\mu s]$, at position $r=10.5$ cm for regime A (left), and position $r=3.5$ cm for regime B (right). A burst is considered as such when the fluctuation overcomes $3\sigma_n$ (i.e., $g>3$) for case A and is lower than $-3\sigma_n$ (i.e., $g<-3$) for case B. The signal is averaged over all events present in the time series.

of the two samples. The average shape of bursts displays a full width at half maximum (FWHM) of about 30 μs and it is asymmetric for regime A. For regime B, the hole turns out to be more symmetric with a FWHM of about 120 μs.

According to Ref. [20], the large positive events in case A are driven by a Rayleigh-Taylor-like instability, triggered by a centrifugal acceleration. An alternative explanation is that of a sheath instability [3]. In regime B, the negative events seem to be related to slower reactions occurring in the plasma bulk. Here, the onset of the instability could be due to a particle drift [29], this in keeping with the observed conspicuous radial ion diffusivity.

The elapsed (waiting) time between two successive bursts $\Delta\tau$ has been determined for the same positions considered in Fig. 9. The corresponding PDFs are plotted in Fig. 10. The PDFs have been smoothed over bins of increasing width $W_k(\alpha)=\alpha^k\Delta t$, where $k=0,1,2,\ldots$, $0<\alpha<2$ and Δt is the time sampling. The results reported are independent of the width of the exponential bin α^k used, and more in general, of the chosen threshold.

As is apparent from Fig. 10 both distributions show a dip around $\tau\approx 100$ μs, followed by a broad hump at higher time scales. For both regimes, the time scales $\tau\leqslant 100$ μs are related to the FWHM of the typical intermittent event. It is worth noticing that the "plateaux" observed in the PDFs at larger time scales, $\tau>100$ μs, correspond to the time intervals where the Hurst exponents have been determined (see Fig. 7). This suggests that the long-time correlations observed in both regimes are probably related to the time-scale invariance between bursts. This behavior is systematically observed for all the radial positions displaying intermittency.

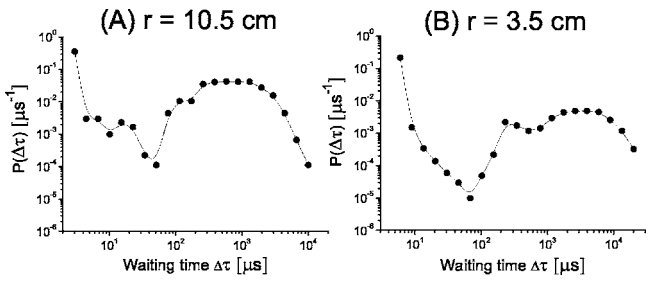

FIG. 10. The PDF of waiting times $\Delta\tau$ $[\mu s]$ between successive bursts, at position $r=10.5$ cm for regime A (left panel), and position $r=3.5$ cm for regime B (right panel) are shown. The continuous line is plotted as a guide.

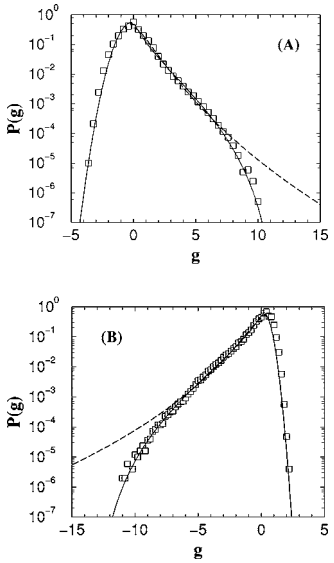

FIG. 11. The PDF $P(g)$ for density fluctuations vs scaled variable $g=\tilde{n}_e/\sigma_n$ for: (a) regime A at a distance $r=10.5$ cm (open squares) and (b) regime B at a distance $r=3.5$ cm (open squares). The continuous lines are fits to the data according to: (a) Eq. (2) for $0\lesssim g$ with $q=0.81$, $\sigma_1=1.42$, $g_1=0.118$, and $b=0.5$, and $y=b_2\exp[-0.5(g/g_2)^2]$ for $g\lesssim 0$ with $b_2=0.55$ and $g_2=0.75$. (b) Eq. (2) for $g\lesssim 0$ with $q=0.81$, $\sigma_1=1.42$, $g_1=-0.135$, and $b=0.5$, and $y=b_2\exp[-0.5(g/g_2)^2]$ for $0\lesssim g$ with $b_2=0.65$ and $g_2=0.40$. The dashed lines are log-normal fits, Eq. (1), with: (a) $a=0.36$, $\sigma_0=0.53$ and $g_0=1$ for $g>1$; (b) $a=0.45$, $\sigma_0=0.63$ and $g_0=-0.8$, for $g<-1$.

C. Fat-tails of intermittent PDFs

It is interesting to study the PDF of scaled density fluctuations, $g=\tilde{n}_e(r,t)/\sigma_n$, for the signals shown in Fig. 2. These are shown in Fig. 11, where the long tail of the PDF occurs for positive g in regime A, and for negative g in regime B. It is interesting to note that both shapes are indeed quite similar regardless of the type of regime and type of instability.

The question arises of how to characterize the shape of the PDF. One possibility is to consider a log-normal dependence, as suggested for the density PDF at the border of several fusion devices (see, e.g., Ref. [12]). The standard log-normal function has the functional form

$$P(g) = a\exp\left[-\frac{1}{2\sigma_0^2}\left(\ln\frac{g}{g_0}\right)^2\right], \qquad (1)$$

where a, σ_0, and g_0 are the three parameters for fitting. The first is related to the normalization of the distribution, the second one to its width, and the third one to the location of its maximum. The log-normal form, Eq. (1), approximates well the density PDF around its center but fails at the extreme part of the long tails (dashed lines in Fig. 11). The short-tail parts seem to be consistent with a Gaussian shape.

This asymmetric behavior of the PDF is typical of turbulence intermittency in tokamaks SOL (see, e.g., Ref. [11]), in which a Gaussian shape is also observed in the nonbursty side of the distribution.

In the following, we propose a generalization of the log-normal fit based on the Tsallis' statistics (see Ref. [30] as a general review). The key idea for generalizing Eq. (1) is to write the exponential function as the limiting form in which a new parameter q appears. In the literature it has been referred to as "q-exponential" [30]. In our case we apply it to the log-normal distribution. For the long-tail parts of the PDF we then write,

$$P(g) = b\left[1 - \frac{(1-q)}{2\sigma_1^2}\left(\ln\frac{g}{g_1}\right)^2\right]^{1/(1-q)}, \qquad (2)$$

where b, σ_1, g_1, and q are the four parameters for fitting. The first three parameters have the same meaning as the previous ones. The new parameter q plays the role of the Tsallis' entropic index. If $q \to 1$, Eq. (2) reduces back to the standard log-normal function Eq. (1). The functional shape reported in Eq. (2) is very close to the one proposed for ordinary turbulence [31,32]. As is apparent from Fig. 11, a satisfactory fit is obtained using the modified log-normal Eq. (2).

IV. CONCLUSIONS

In a magnetized rotating plasma column, two turbulent regimes are observed which turn out to be qualitatively different. They are obtained by changing the plasma boundary conditions, namely, the collecting potential V_{plate}. The first one corresponds to a turbulent slowly rotating column (regime A) in which there exists a velocity shear-layer sharply separating the bulk plasma from the edge region. The former rotates nearly as a rigid body, while in the latter a strong intermittency occurs. In regime B, the column rotates even slower. The plasma bulk loses part of its coherence and displays intermittency, while in the edge region density fluctuations show standard diffusive behavior as opposed to the super-diffusivity observed in the previous case A.

In regime A, the detaching structures present at the border of the plasma column [20] and the velocity profiles (Fig. 6), seem to induce a super-diffusive process of density fluctuations in the edge region. This is consistent with the observed typical bursts and their waiting time PDF. In regime B, it is interesting to note that in the plasma bulk a subdiffusion takes place together with the presence of negative intermittent events (holes). The phenomenology in the latter needs further investigations.

A modified log-normal distribution seems to fit appropriately the fat-tailed density PDF, with a Tsallis' index $q = 0.81$. The functional form provided by Eq. (2) should not be intended as a definitive description of the intermittent density PDF. Rather, it is a first attempt to introduce the concept related to generalized statistics in plasma-turbulence context, as recently discussed for ordinary fluid turbulence [31–33].

ACKNOWLEDGMENTS

S.M. wants to thank the people of PIIM research group for the kind hospitality during his stay in Marseille. We would like to thank A. Fredriksen for suggestions raised on the manuscript, and J. J. Rasmussen, A. V. Chechkin, and S. I. Krasheninnikov for fruitful discussions.

APPENDIX: WAVELET FLUCTUATION ANALYSIS

The existence of possible long-time correlations in turbulent signals can be searched through the determination of the Hurst (H) exponent of the corresponding time series. Many methods have been considered in the plasma literature to calculate H, with different degrees of accuracy and success (see Ref. [7] as a general review). Recently, wavelets analysis to compute H has been applied to fluctuating signals taken from a simple magnetized torus [19]. The wavelet analysis has been designed to eliminate the effects of possible trends, which could affect the estimation of H. Its name is due to the use of Haar's wavelets in building the fluctuation functions [see Eqs. (A3)–(A5) below] (see, e.g., Ref. [34]).

In this technique, we regard the fluctuating signal as steps performed by a random walker along a one-dimensional path, where its position after t time steps is obtained as

$$Y(t_i) = \sum_{k=1}^{i} X(t_k), \quad t_i = i\Delta t, \quad 1 < i \leqslant N, \qquad (A1)$$

where $X(t)$ is the discrete, zero-mean time series with N values. The quantity $Y(t)$ plays the role of the profile associated to a fractional Brownian motion (FBM), which is a paradigmatic model for long-range correlated walks [35]. For a typical example of a fluctuating profile see Fig. 1 in Ref. [19].

Then, we average $Y(t)$ over nonoverlapping time intervals of length $\ell = \tau/\Delta t$, where $\tau \geqslant \Delta t$ is the time-grain scale at which fluctuations are studied, yielding

$$W_n(\ell) = \frac{1}{\ell}\sum_{j=1}^{\ell} Y(t_{(n-1)\ell+j}), \quad \ell \geqslant 1, \qquad (A2)$$

with $1 \leqslant n \leqslant \text{int}(N/\ell)$, from which we evaluate the fluctuations of such coarse-grained walks, denoted as first-order wavelets, according to

$$F_1^2(\ell) = \langle [W_{n+1}(\ell) - W_n(\ell)]^2 \rangle, \qquad (A3)$$

where $\langle \cdots \rangle$ denotes the average taken over all consecutive intervals $(n, n+1)$. The exponent H can be estimated from the expected scaling relation $F_1(\ell) \propto \ell^{\text{H}}$. To disentangle intrinsic fluctuations from the presence of possible trends in the signal, one can also study higher-order wavelets, such as

$$F_2^2(\ell) = \langle [W_{n+2}(\ell) - 2W_{n+1}(\ell) + W_n(\ell)]^2 \rangle, \qquad (A4)$$

$$F_3^2(\ell) = \langle [W_{n+3}(\ell) - 3W_{n+2}(\ell) + 3W_{n+1}(\ell) - W_n(\ell)]^2 \rangle, \tag{A5}$$

where the averages $\langle \cdots \rangle$ are performed on consecutive triplets $(n, n+1, n+2)$ and quadruplets $(n, n+1, n+2, n+3)$, respectively.

The Hurst exponent carries important information about the diffusivity of the observable related to the signal $X(t)$. The general theory of the FBM [35] predicts that the temporal behavior of the second moment of $X(t)$ scales versus time τ as,

$$\langle X^2(t) \rangle_\tau \propto \tau^\mu, \tag{A6}$$

where $\langle \cdots \rangle_\tau$ is the average taken on the time span $(0, \tau)$ of many repetitions of the signal, $\mu = 2\mathrm{H}$ is the diffusion exponent ($0 \leqslant \mu \leqslant 2$). If $0 \leqslant \mathrm{H} < 0.5$ the quantity $X(t)$ is said to be subdiffusive, if $\mathrm{H} = 0.5$ it displays standard diffusion, if $0.5 < \mathrm{H} \leqslant 1$ one is observing a super diffusive process.

[1] F. F. Chen, Phys. Rev. Lett. **9**, 333 (1962).
[2] F. F. Chen, Phys. Fluids **9**, 2534 (1966).
[3] F. F. Chen, Phys. Fluids **8**, 752 (1965).
[4] S. S. Moiseev, and R. Z. Sagdeev, Sov. Phys. JETP **17**, 515 (1964).
[5] F. F. Chen, Phys. Fluids **8**, 1323 (1965).
[6] B. A. Carreras, B. van Milligen, M. A. Pedrosa, R. Balbín, C. Hidalgo, D. E. Newman, E. Sánchez, M. Frances, I. García-Cortés, J. Bleuel, M. Endler, S. Davies, and G. F. Matthews, Phys. Rev. Lett. **80**, 4438 (1998).
[7] B. A. Carreras, B. van Milligen, M. A. Pedrosa, R. Balbín, C. Hidalgo, D. E. Newman, R. Bravenec, E. Sánchez, G. R. McKee, I. García-Cortés, J. Bleuel, M. Endler, C. Riccardi, S. Davis, G. F. Matthews, E. Martines, and V. Antoni, Phys. Plasmas **6**, 1885 (1999).
[8] C. X. Yu, M. Gilmore, W. A. Peebles, and T. L. Rhodes, Phys. Plasmas **10**, 2772 (2003).
[9] G. M. Zaslavsky, M. Endelman, H. Weitzner, B. A. Carreras, G. McKee, R. Bravenec, and R. Fonk, Phys. Plasmas **7**, 3691 (2000).
[10] E. Sánchez, C. Hidalgo, D. López-Bruna, I. García-Cortés, R. Balbín, M. A. Pedrosa, B. van Milligen, C. Riccardi, G. Chiodini, J. Bleuel, M. Endler, B. A. Carreras, and D. E. Newman, Phys. Plasmas **7**, 1408 (2000).
[11] G. Y. Antar, S. I. Krasheninnikov, P. Devynck, R. P. Doerner, E. M. Hollmann, J. A. Boedo, S. C. Luckhardt, and R. W. Conn, Phys. Rev. Lett. **87**, 065001 (2001).
[12] F. Sattin, N. Vianello, and M. Valisa, Phys. Plasmas **11**, 5032 (2004).
[13] D. del-Castillo-Negrete, B. A. Carreras, and V. E. Lynch, Phys. Rev. Lett. **91**, 018302 (2003).
[14] V. Naulin, J. J. Rasmussen, and J. Nycander, Phys. Plasmas **10**, 1075 (2003).
[15] B. Ph. van Milligen, E. Sánchez, and B. A. Carreras, Phys. Plasmas **11**, 2272 (2004).
[16] D. del Castillo Negrete, B. A. Carreras, and V. E. Lynch, Phys. Plasmas **11**, 3854 (2004).
[17] Th. Pierre, H. Klostermann, E. Floriani, and R. Lima, Phys. Rev. E **62**, 7241 (2000).
[18] G. Y. Antar, G. Counsell, Y. Yu, B. Labombard, and P. Devynck, Phys. Plasmas **10**, 419 (2003).
[19] S. Magni, C. Riccardi, and H. E. Roman, Phys. Plasmas **11**, 4564 (2004).
[20] Th. Pierre, A. Escarguel, D. Guymarc'h, R. Barni, and C. Riccardi, Phys. Rev. Lett. **92**, 065004 (2004).
[21] S. I. Krasheninnikov, Phys. Lett. A **283**, 368 (2001).
[22] Th. Pierre, F. Braun, and G. Leclert, Rev. Sci. Instrum. **58**, 6 (1987).
[23] M. Matsukuma, Th. Pierre, A. Escarguel, D. Guyomarc'h, G. Leclert, F. Brochard, E. Gravier, and Y. Kawai, Phys. Lett. A **314**, 163 (2003).
[24] J. L. Terry, S. J. Zweben, K. Hallatschek, B. Labombard, R. J. Maqueda, B. Bai, C. J. Boswell, M. Greenwald, D. Kopon, W. M. Nevins, C. S. Pitcher, B. N. Rogers, D. P. Stotler, and X. Q. Xu, Phys. Plasmas **10**, 1739 (2003).
[25] C. Riccardi, D. Xuantong, M. Salierno, L. Gamberale, and M. Fontanesi, Phys. Plasmas **4**, 3749 (1997).
[26] A. Fredriksen, C. Riccardi, L. Cartegni, D. Draghi, R. Trasarti-Battistoni, and H. E. Roman, Phys. Plasmas **10**, 4335 (2003).
[27] A. Fredriksen, C. Riccardi, L. Cartegni, D. Draghi, R. Trasarti-Battistoni, and H. E. Roman, Phys. Plasmas **11**, 3683 (2003).
[28] A. Fredriksen, C. Riccardi, L. Cartegni, and H. L. Pécseli, Plasma Phys. Controlled Fusion **45**, 721 (2003).
[29] W. Horton, Rev. Mod. Phys. **71**, 735 (1999).
[30] C. Tsallis, Physica D **193**, 3 (2004).
[31] T. Arimitsu, and N. Arimitsu, Physica A **305**, 218 (2002).
[32] T. Arimitsu, and N. Arimitsu, AIP Conf. Proc. **695**, 135 (2003).
[33] T. Arimitsu, and N. Arimitsu, Phys. Rev. E **61**, 3237 (2000).
[34] J. W. Kantelhardt, H. E. Roman, and M. Greiner, Physica A **220**, 219 (1995).
[35] J. Feder, *Fractals* (Plenum, New York, 1988).